Bulgarian Chemical Communications, Volume 48, Special Issue D (pp. 89 – 96) 2016

The effect of nitrate ions on the electrodeposition of PbS semiconducting film: electrochemical and surface analysis

A. Lorparizangen[1*], M. Jafarian[1], F. Gobal[2], S. Miandari[1], M.G. Mahjani[1]

[1]*Department of Chemistry, K.N. Toosi University of Technology, P.O. Box 15875–4416, Tehran, Iran*
[2]*Department of Chemistry, Sharif University of Technology, P.O. Box 11365-9516, Tehran, Iran*

Received June 26, 2016; Revised September 10, 2016

The aggressive effect of NO_3^- ion, present in electrolyte solvent, on the electrodeposition of PbS film was studied by cyclic voltammetry (CV), cyclic potentiodynamic polarization (CP), and electrochemical impedance spectroscopy (EIS) methods. The CV curves confirmed that presence of NO_3^- 0.1 M in the solution leads to a dramatic increase in amplitude of current and considerable damage to the passive layer at breakdown potential (E_b) of 0.16 V/SCE. Cyclic polarization studies revealed that I_{corr} goes up from 44.08 μA/cm^2 to 551 μA/cm^2 as NO_3^- concentration increases from 0.05 M to 2 M. However, 0.01 M NO_3^- solution notably improved passivation of PbS thin films. The capacitive semicircle with low R_{ct} at medium frequency in the Nyquist plot, indicated structural change in passive layer (PbS film) and pitting corrosion on its surface. X-ray diffraction (XRD) and scanning electron microscopy (SEM) were used to investigate the aggressive behavior of NO_3^- and deformation of the surface.

Keywords: Lead sulfide;cyclic polarization; electrochemical impedance spectroscopy; pitting corrosion

INTRODUCTION

Lead sulfide (PbS) is a well-known semiconductor with a narrow band gap of 0.41 eV and relatively large excitation Bohr radius[1-3]. These characteristics make it a basic industrial material. Lead sulfide has been widely used in many areas such as infrared detection applications, Pb2+ ion selective sensor, solar energy absorption, photography, photo resistors, and diode lasers [1-3].

PbS thin film is deposited by various deposition methods which are basically categorized into two maintypes:

1) electrochemical [3-6] and

2) chemical [4-8] methods. Extensive research has been devoted to production of PbS thin film by various electrodeposition techniques. Unlike routine deposition methods, electrodeposition approach provides advantages such as operation at ambient temperature and pressure [9, 10], low cost, and easy control of thickness of the film [11].

So far several studies on the electrodeposition of PbS in a variety of electrolytes have been carried out [6] and considerable effort has been focused on PbS propertiesin different media [12-15] using a wide variety of electrochemical methods. However, there arefew reports on the effect of electrolytes on the PbS layer and its corrosion in aqueous media. Semiconducting properties of PbS films are adversely influenced by aggressive ions .PbS films are susceptible to corrosion as PbS becomes oxidized. This process is depicted in the Pourbaix diagram for the lead/water system [7, 12, 15]. Recently, the aggressive effects of NO_3^- ions on aluminum rods [16] and stainless steel [16] have been studied. The aggressive nature of NO_3^- in the corrosion of Pb in different media has also been reported [16-18].

In this work, we have studied the influence of KNO_3 solution on deposition of PbS in sodium sulfide medium and found its optimum concentration. We investigate the effects of NO_3^- on breakdown and structural change of the passive film. Cyclic voltammetry, chronoamperometry, and electrochemical impedance spectroscopy methods were used to characterize the mechanism of this process in detail. These studies were accompanied by surface analysis methods, i.e. XRD and SEM [19].

EXPERIMENTAL

Sodium sulfide, potassium nitrate, and potassium hydroxide used in this work were Merck products of analytical grade and were used without further purification. Electrochemical studies were carried out in a conventional three electrode cell powered by an electrochemical system comprising of a potentiostat/galvanostat (EG&G, model 273A) controlled by a PC through M270 and M398 software (GPIB interface), and a frequency response analyzer (EG&G, model 1025). The frequency range of 100 kHz – 10 MHz and modulation amplitude of 5mV were employed in electrochemical impedance studies. The working

* To whom all correspondence should be sent:
E-mail: aminlorpari@yahoo.com

electrode employed in the present study was made of very pure lead rod (purity 99.999%, w/w of Pb) in shape of a cylindrical rod, welded to Cu wire for electrical contact, and mounted to expose 1cm^2 area to the electrolyte. Graphite as a counter electrode, and a saturated calomel electrode (SCE) as a reference electrode were used. Prior to each experiment, the surface pre-treatment of the working electrode was performed by mechanical polishing of the electrode surface with successive grades of emery papers down to 2000 grit. The electrode was rinsed with ethanol and distilled water and then was dipped in the electrolyte. All the electrochemical experiments were performed at room temperature.

XRD analysis was performed on X-Pert pro MPD (PAN analytical) diffractometer with CuK α radiation (λ= 1.5406A°) in the 2θ range of 10 to 90°.

SEM images were created using the electrode surface after potentiostatic polarization at the potential of 0.55 V for 60s.SEM examinations were performed by a TESCAN (model VEGA-TS 5136MM) electron microscope using various magnifications to observe different aspects of the surface.

RESULTS AND DISCUSSION

Cyclic voltammetry

The potentiodynamic studies of Pb electrode were performed in three different solutions: 1) 0.1 M Na_2S, 2) 0.1 M Na_2S mixed with 0.1M KNO_3, and 3) 0.1 M Na_2S mixed with 0.1 M NaOH. The potential was swept from -2 to 2 V/SCE at the sweep rate of 50 mV/s. The potential was then swept back for a second time from 2 to -2 V/SCE at the same rate. Fig. 1(a,a′) presents the cyclic voltammogram of Pb electrode in Na_2S solution with two anodic peaks at -0.2 and 1.3 V/SCE. First peak (A_1) was observed in potential region of -0.4 to 0.2 V/SCE, (Fig. 1a′). This potential region is related to oxidation of Pb to $Pb^{2+}$and formation of PbS as reported by Yang et al[19]. Second peak (A_2) was in potential region of 0.4 to 1.4 V/SCE (Fig. 1a). Passive region is formed from -0.25 to 1.3 V/SCE. At potential of 1.3 V, the oxygen evolution on the Pb surface leads to removal of PbS film from the surface, which in turn prevents the passivation of the electrode [20, 21]. Therefore, the second anodic peak enhances passivity breakdown of the layer at a certain potential (breakdown potential, E_b) [14]. The cyclic voltammograms show that the A_2 peak rises more upon addition of NO_3^- than OH^-. In contrast, A_1 peak does not demonstrate considerable change upon addition of either NO_3^- than OH^-.

These observations confirm that despite the stability of the highly adhesive PbS film, formation of PbO results in breakdown of the passive PbS film [14].Since the solubility constant of PbS is approximately 10^8 times less than that of $Pb(OH)_2$, ($K_{sp}=1.42\times10^{-20}$) formation of oxide layers is not expected. XRD results confirm formation of PbO and $Pb_3O_2(OH)_2$ layers. Reactions involved in formation of PbO are described below[20].

$$Pb + 2OH^- \longrightarrow Pb(OH)_2 + 2e \ , \qquad (1)$$

$$Pb(OH)_2 \longrightarrow PbO + H_2O \ , \qquad (2)$$

Fig.1b shows the effect of addition of NO_3^- solution with different concentrations on the passivation of PbS. Increasing the concentration of NO_3^- caused no significant change in the first anodic peak, however, the second anodic peak raised markedly. Upon addition of 0.01 M NO_3^- solution, the passive region spanned a relatively wide range of potential. Upward shift of curve 2, reflecting a slight increase in current density, is due to higher conductivity of electrolyte solution. An increase in nitrate concentration up to 0.05 M created an E_b at 0.41 V/SCE and caused the anodic current to increase. Further increase in the NO_3^- concentration caused E_b to shift to more negative potentials (E_b=0.16 V/SCE in 0.1M). The current density increased as well.

In 0.01 M and 0.05 M NO_3^- solutions the cathodic curve was found at higher current density level than the anodic curve (Fig. 1b′). In contrast, in 0.1 M NO_3^- solution the cathodic curve was found in lower current density level than the anodic curve. This difference indicates that the passive layer was significantly damaged at nitrate concentration of0.1 M [16, 22].

Formation of a large anodic peak with a high current density level in the potential range between PbS formation potential (-0.2V/SCE) and O_2 evolution potential (1.3V/SCE) indicates the aggressive effect of NO_3^- on PbS passive layer (Fig. 1b). This effect is further confirmed by the displacement of E_b potential toward formation potential of PbS, and conversion of the anodic peaks to a single peak. Lower value of repassivation potential (E_{rep}) compared to breakdown potential (E_b) indicates cessation of pit growth in PbS passive layer, and formation of lead oxide and lead hydroxide compounds in PbS film layer [23].

In order to recognize the effectiveness of NO_3^- in causing pits in the film layer, breakdown potential versus the logarithmic concentration of NO_3^- was plotted (Fig. 1c). The aggressive behavior

of a given anion is more prominent if the curve representing equation (3) is close to a straight line [22, 24]. The value of B for NO_3^- was 0.526.The relationship between E_b and logarithmic concentration of NO_3^- was found to be linear which suggests the aggressive behavior of NO_3^- ions.

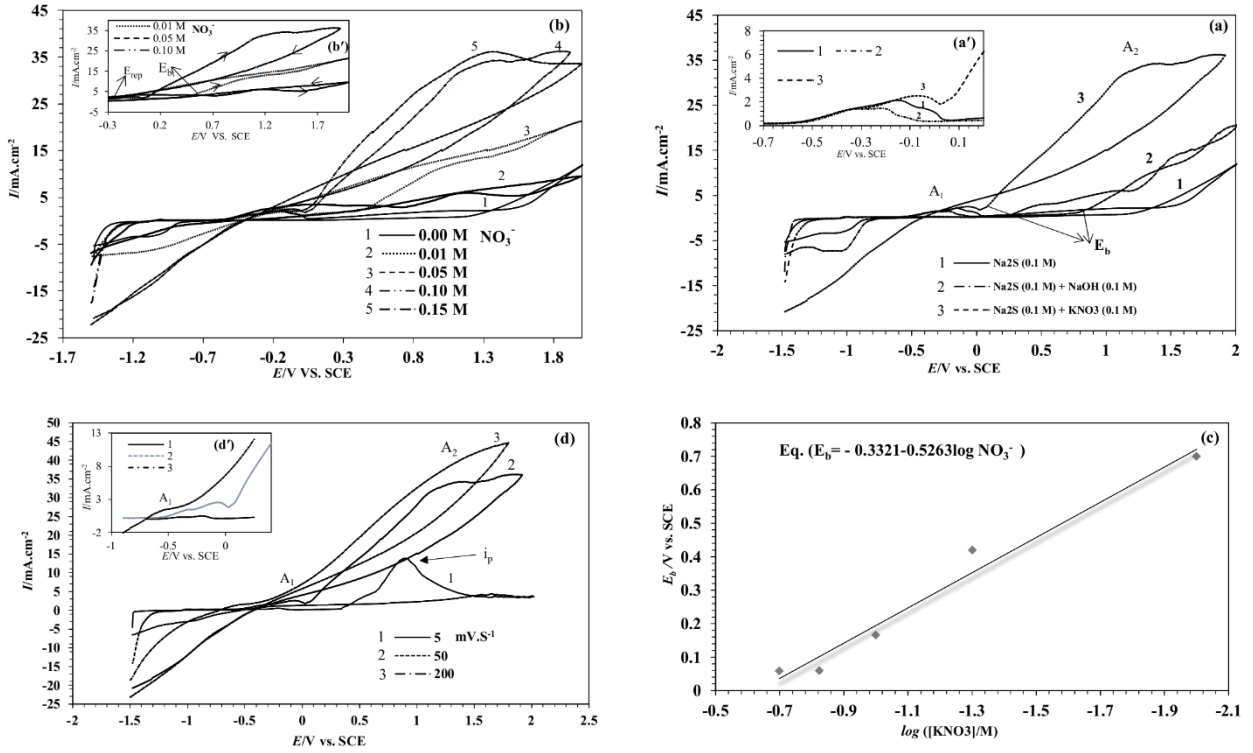

Fig. 1. Cyclic voltammograms for Pb electrode (a) in three different media with scan rate of 50 mV/s (b) in solution containing Na2S and different concentrations of 0.0 – 0.15 M (c) in 0.1 M Na2S + 0.1 M KNO3 mixed solution at different scan rates of 5, 50 and 200 mV/s (d) Plot of pitting potentials versus log [ ]

$$E_b = A - B \log C_x , \quad (3)$$

A and B are constants and C_x is the concentration of aggressive ion. E_b, critical breakdown potential, is th potential above which film breakdown occurs [23-25].

The influence of scan rate (5, 50, and 200 mV/s) on the potentiodynamic polarization curves of Pbin a solution withNa_2S concentration of 0.1 M and KNO_3 concentration of 0.1M was studied. As scan rate increased, the anodic peak current density (i_p) shifted toward more positive values (Fig. 1d) and the potential value of A_1 peak shifted toward more negative values (Fig. 1d′).

A_1peak in Fig. (2a) shows the formation of PbS in the Na_2S solution. With increasing scan rate, i_p went up. Nevertheless, the PbS formation peak in Na_2S+KNO_3 solution (A_1) did not exhibit a significant change. In reverse scan, reduction peaksC_1 (-0.8 V/SCE) and C_2 (-1.3 V/SCE) were generated by reduction of compounds were oxidized in A_2 and A_1, respectively. As the scan rate increased, C_1 tended to overlap with C_2 to make a single peak. This overlap is thought to be due to rapid formation of a solid layer of PbS (K_{sp}=3.0×10^{-28}) according to the following reaction:

$$Pb + S^{2-} \longrightarrow PbS + 2e , \quad (4)$$

Fig. (2a′) shows the linear dependency of anodic peak current density (i_p) on the square root of scan rate ($v^{1/2}$) [26]. Fairly straight lines with correlation coefficients of 0.98were been obtained suggesting that diffusion of reacting species dominantly control the kinetics of anodic processes [27].

Chronoamperometry studies

The pitting corrosion effect of NO_3^- can be related to the adsorption competition between NO_3^- and S^{2-} ions on the PbS surface sites. We attempted to verify this assumption by applying potentiostatic methods at the potential of the second anodic peak (0.55 V/SCE) for 60 s.

Fig. (2b) shows the chronoamperograms of lead electrode in three different electrolytes. Curves 1 and 2 show a decreases in current density. The reason is nucleation of the passive layer [28] and continued S^{2-} flux. This nucleation process led to thinning of PbS layer. In other words, the oxidation

process was overtaken by slow mass transfer to the surface. The current densities in curves 1&2 are smaller than that incurve 3 due to mass transfer limitations of different electrolytes. An increase in the current density in the presence of NO_3^- as an aggressive anion (curve 3) corresponds closely to passivity breakdown of the passive film at early stages of the process (pit growth time) [29]. The passive layer was partially re-established. Polarization gradually caused a decrease in current density according to the ohm law, V= IR, where R is the electrical resistance of the electrolyte plus any passive film inside of pit region. IR drop was thus related to the potential difference between the pit bottom at metal interface and the passive surface [16]. Fluctuations of corrosion current in curve 3 confirmed that the flaws were present in the film.

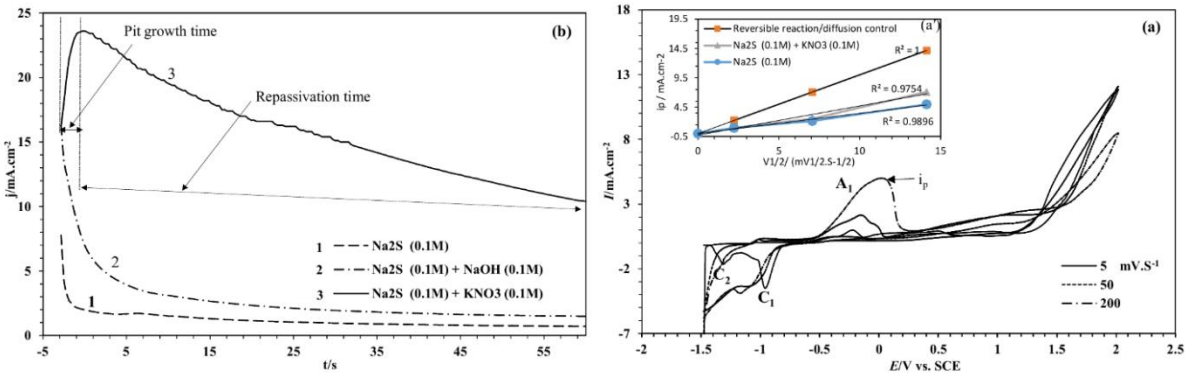

Fig. 2. (a)Cyclic Voltammograms for Pb electrode in 0.1 M Na2S solution between -1.5 and 2 V/SCE at different scan rates of 5, 50 and 200 mV/s.(b) Chronoamperograms of lead electrode in different electrolytes, Eapply=0.55.

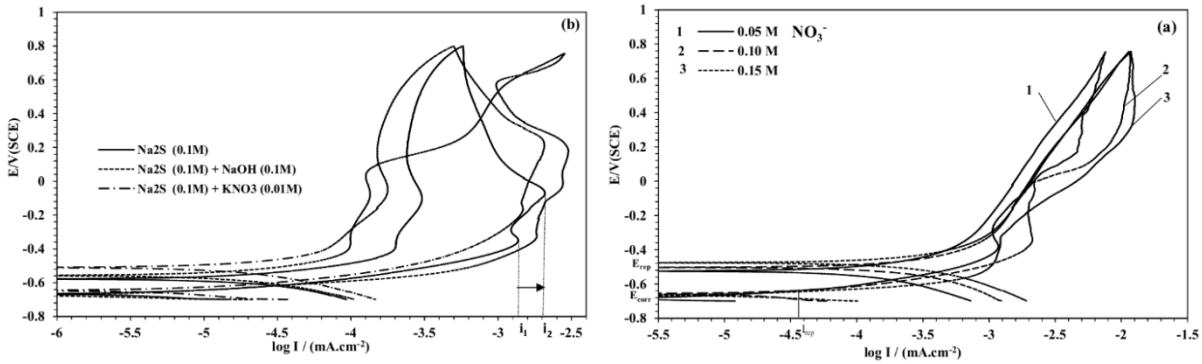

Fig. 3. Cyclic polarization curve of PbS in different media (a) without aggressive effect (b) with aggressive effect.

Cyclic potentiodynamic polarization

Fig. (3a) shows the cyclic polarization curves of the potentiodynamically deposited thin film layers on thePb electrode in three different electrolytes. In all cases, the cyclic polarization curves were swept between -700 to 750 mV with 10 mV/s scan rate. The cyclic polarization curve of 0.1 M Na_2S solution exhibited the corrosion potential (E_{corr}) of -668 mV/SCE and corrosion current density (I_{corr}) of 30.44 μA/cm^2. The cyclic polarization curve of 0.1 M Na_2S+0.1 M NaOH solution yielded E_{corr} of -674 mV/SCE and I_{corr} of 81.12 μA/cm^2. In 0.01M NO_3^- solution, E_{corr} and I_{corr} were -647mV/SCE and 44.08μA/cm^2, respectively.

These data show an increase in I_{corr} which was not due to pit formation on the surface of PbS layer. Based on [16], we concluded that incorporation of water molecules into the PbS passive film formed concentration gradients across metal-film and film-solution interfaces. These gradients caused flaws in the passive layer which increased the critical current density from i_1 to i_2 [30], (Fig. 3a).

Upon addition of 0.01 M NO_3^- solution to Na_2S solution, NO_3^- ions help to distribute the current, generated in the flaws, all over the passive film. Thus, a film forms on the uniformly polarized surface at higher potentials. An increase in concentration of NO_3^- to 0.05M makes the passive film unstable (Fig. 3b). This can lead to localized corrosion on the PbS surface. Dissolution of passive layer advances a flaw to a pit [16]. Upon addition of 0.1 M NO_3^- solution, E_{corr} and I_{corr} measured -658 mV/SCE and 0.15 mA/cm^2, respectively. Value of I_{corr} in case of addition of NO_3^- to Na_2S solution was 2 to 5 times larger than addition of OH^-. An increase in the value of pitting current density (I_{pit}) confirms that the film did not have a stable passive state. The corrosion, passivation, breakdown, and re-passivation

parameters are calculated by the cyclic polarization method and are summarized in the paper.

The 0.1M solution of OH^- showed a large hysteresis loop (Fig.3a). Crevice corrosion did not propagate immediately after corrosion initiation at -118 V which resulted in surface polarization andsubsequent formation of passive layer on the surface. This layer was found to be compact and favorable because it contains $Pb(OH)_2$ formed according to the following reactions:

$$\frac{1}{2}O_2+H_2O+2e\longrightarrow 2OH^-, \quad (5)$$

$$Pb^{2+}+2OH^-\longrightarrow Pb(OH)_2, \quad (6)$$

Moreover, hysteresis loop was larger in 0.1 M OH^- curve (Fig.8) than 0.1 M NO_3^- curve (Fig.3b). This observation indicates that NO_3^- causes a larger increase in the current, although the conductivity of NO_3^- and $OH^-$are close.

Electrochemical impedance spectroscopy

Typical Nyquist and Bode-phase plots are presented in Fig. 4a,b. Curve 1 is plotted forthe Pb electrode in the Na_2S solution. It has one capacitive loop with a resistance value of about 400 $\Omega.cm^{-2}$ against the charge transfer process for deposited PbS film. Value of charge transfer resistance was found to be very large when the OH^- anions were added to Na_2S solution (Nyquist plots, curve 2) which was due to the formation of stable and compact passive film in the solution. This result is in accordance with the cyclic polarization studies (Fig. 3a).In the corresponding Bode-phase plot (Fig. 4b, curve 2) the capacitive response was observed with 60 degree phase angle in the intermediate frequencies. Addition of NO_3^- ions resulted in two overlapping capacitive loops (curve 3).At high frequencies, semicircle of NO_3^- solution curve was smaller than those of NO_3^--free solution and NO_3^-+OH^- solution which was owing to decreased stability of passive layer and increased porosity of the film. Nitrate ions penetrated the passive film [31] and caused structural changes in the surface which in turn led to a remarkable decrease in diameter of the semicircle (R_{ct}). Nitrate anions were then adsorbed on the film-solution interface at OCP. This behavior is shown in the Bode-phase spectrum (Fig.4b, curve 3) with the phase value of 20 degrees in high frequencies. The PbS layer was then removed and lead oxide layer was formed. Small values of second charge transfer resistance (25 $\Omega.cm^{-2}$) and phase (10 degrees) indicate low resistivity and high permeability of the passive film which is owing to the formation of lead oxide. In addition, the presence of one inductive loop at low frequency range indicates that the pitting process occurred on the surface after passivation process [32].However, [33] mentioned an inductive loop associated with the synchronized adsorption↔desorption process (i.e. adsorption of lead oxide ↔ desorption of lead sulfide).Our experimental data revealed the aggressive effects of NO_3^-culminating in structural change and pitting corrosion of passive layer (PbS film) .

Nitrate, as a chaotropic anion [34] with a weak electric field, can become adsorbed on or even penetrate into the film-solution interface. Hydroxylic ion is a chosmotropic anion with a strong electric field at short distance [35]. Therefore, $OH^-$was less likely than $NO_3^-$to be adsorbed on the passive film-solution interface which resulted in generation of more cation vacancies that migrate to the metal-film interface [36].

X-ray diffraction studies

Fig. 5 shows XRD pattern of the product prepared potentiostatically on the Pb surface ina 0.1M Na_2S + 0.1M KNO_3solution in 60 s. The XRD pattern demonstrated the presence of $H_2Pb_3O_4$ with tetragonal structure (JCPDS card no.77-1895), PbO with orthorhombic structure (JCPDS card no.77-1971), and PbS with cubic crystal structure (JCPDS card no.78-1057). PbO was detected in the passive layer according to the XRD pattern of the film (Fig.5).

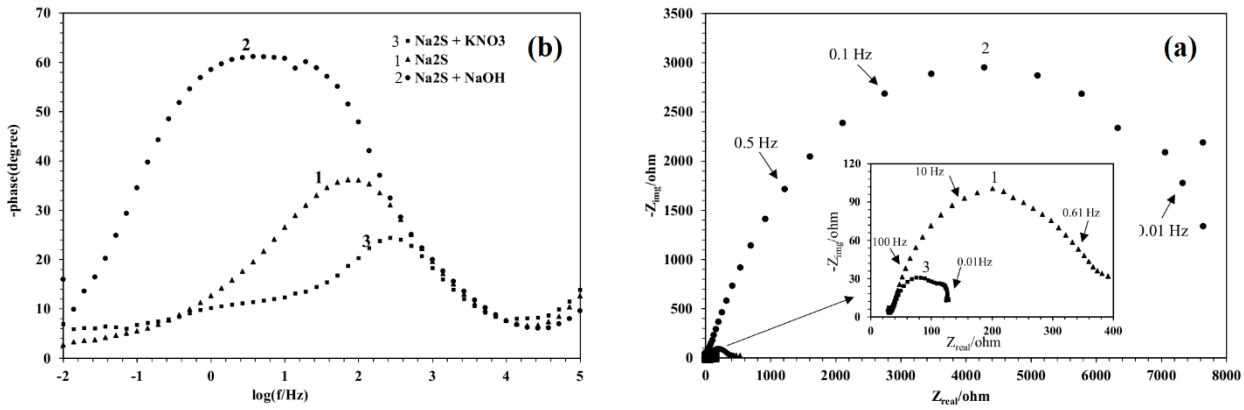

Fig. 4. a) Nyquist plots and b) Bode-Phase spectra of deposited passive film in solutions containing 0.1 M concentration of different electrolytes, at the OCP.

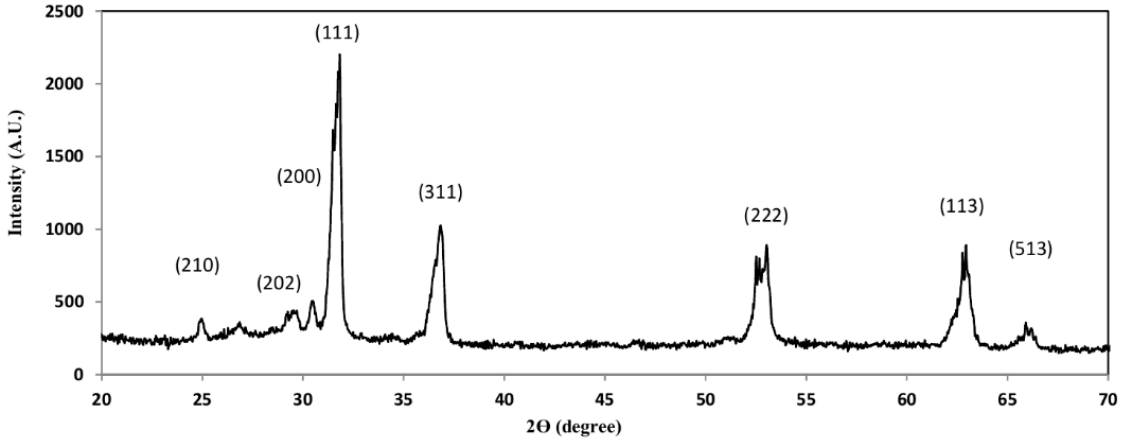

Fig. 5. XRD pattern of potentiostatically oxidized Pb electrode in 0.1 M Na_2S+0.1 M KNO_3 solution at 0.55 V/SCE.

Reduction of NO_3^- is thermodynamically easier than Pb^{2+} in the potential used in our experiment (0.55 V/SCE) because of the fact that reduction potential of NO_3^- [$E^{\circ}_{NO_3^-/NO_2^-}$ (-0.234 V/SCE)] is more positive than that of Pb^{2+} [$E^{\circ}_{Pb^{2+}/Pb}$ (-0.36 V/SCE)].

Reduction of NO_3^- leads to the formation of OH^- according to the following reaction,

$$NO_3^- + H_2O + e \rightarrow NO_2^- + 2OH^- \qquad (7)$$

OH^- ions and Pb^{2+}ions were generated at the same time on the surface of anode and cathode respectively. When direct current passed through the electrochemical cell, Pb^{2+}ions reacted with OH^- ions to production of $Pb(OH)_2$, which was then hydrated to form PbO [16].

SEM and morphology of surface

Obtained SEM images (Fig. 6) showed the morphology of the passive film on the Pb surface after potentiostatic treatment in three different solutions: 1) 0.1 M Na_2S, 2) 0.1 M Na_2S mixed with 0.1 M KNO_3, and 3) 0.1 M Na_2S mixed with 0.1 M NaOH. Bare surface of Pb was scanned by SEM (Image a). Electrochemically treated surface of Pb in the pure solution of Na_2S had an uneven surface with no evidence of pitting is observed (Image b). Upon addition of NO_3^- to Na_2S solution, the entire surface of the electrode was damaged and covered with irregular holes (Images c, e). A hole of testicular shape and 5.3×3.5 μm diameter was observed (Image g). PbS surface had superficial defects in case of OH^- solution (Images d, f), whereas the surface was observed to have clear holes in case of NO_3^- solution (Image e). The effect of NO_3^- on the pitting corrosion of passivated thin film was clearly demonstrated in the SEM images.

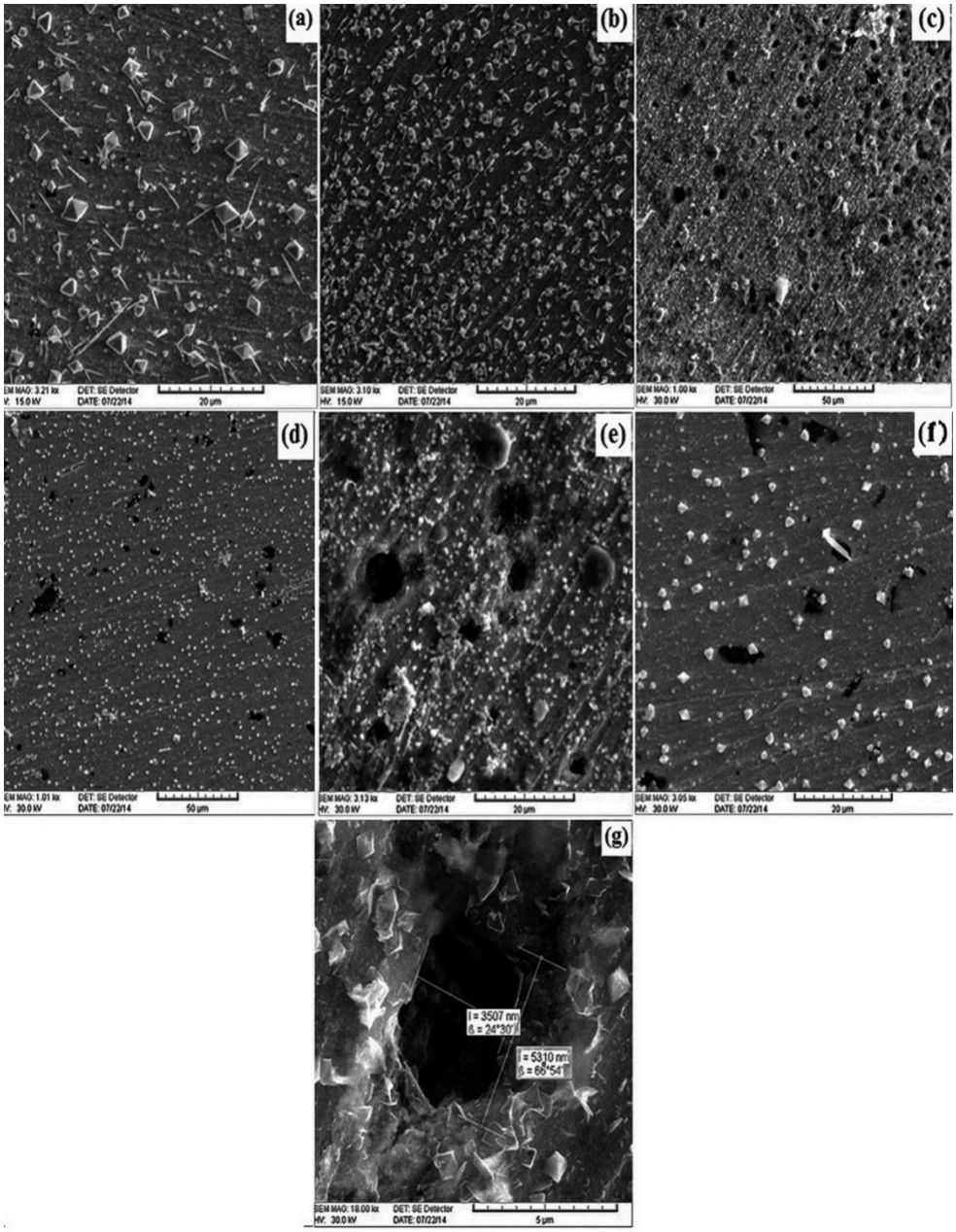

Fig. 6. SEM images of Pb surface (a), and Pb surface after potentiostatic polarization at 0.55 V/SCE for 60 s in 0.1M Na_2S (b), 0.1 M Na_2S+0.1 M KNO_3 (c,e,g) and 0.1 M Na_2S+0.1 M NaOH (d,f) solutions.

CONCLUSIONS

Potentiodynamic polarization of nitrate-free solution exhibited two anodic peaks corresponding to the formation of PbS and oxygen evolution. Addition of NO_3^- ion caused these peaks to merge and induced abrupt increase in current density. This increase is related to more aggressive behavior of NO_3^- in compared with that of optimum concentration of NO_3^- was obtained to be 0.01 M. An increase in the concentration of NO_3^- in sodium sulfide solution to values larger than the optimum induced pitting attack at a certain potential (E_{pit}). The pitting corrosion of PbS increased with increasing NO_3^- concentration. Chrono-amperometric studies revealed an IR drop at the bottom of pit at pit growth initiation. XRD pattern showed deformation of passive film due to aggressive behavior of NO_3^- ions. Three-phase mixture of $H_2Pb_3O_4$, PbO, and PbS and presence of pits on the electrode surface were also confirmed using XRD.

Acknowledgment: *We gratefully acknowledge the support of this work by K.N. Toosi University of Technology Research Council.*

REFERENCES

1. M. Mozafari, F. Moztarzadeh, *J. Colloid Interface Science*, **351,** 442 (2010).
2. M. Barote, A. Yadav, T. Chavan, E. Masumdar, *Digest J. Nanomater. Biostruct.*, **6**, 979 (2011).

3. A. O. Nejo, A. A. Nejo, R. V. Pullabhotla, N. Revaprasadu, *J. Alloys Compounds*, **537**, 19 (2012).
4. A. Aghassi, M. Jafarian, I. Danaee, F. Gobal, M. Mahjani, *J. Electroanal. Chem.*, **661**, 265 (2011).
5. P. Nair, V. Garcia, A. Hernandez, M. Nair, *J. Physics D: Applied Physics*, **24**, 1466 (1991).
6. F. B.E. Nisancı, U.M. Demir, *Langmuir*, **28**, 8571, (2012).
7. M. Alanyalıoğlu, F. Bayrakçeken, Ü. Demir, *Electrochimica Acta*, **54,** 6554 (2009).
8. M. Takahashi, Y. Ohshima, K. Nagata, S. Furuta, *J. Electroanal. Chem.*, **359**, 281 (1993).
9. A. P. Gaiduk, P. I. Gaiduk, A. N. Larsen, *Thin Solid Films*, **516**, 3791 (2008).
10. Z. Zeng, S. Wang, S. Yang, *Chemistry of Materials*, **11**, 1999, 3365.
11. .J. Valenzuela-Jauregui, R. Ramırez-Bon, A. Mendoza-Galvan, M. Sotelo-Lerma, *Thin Solid Films*, **441,** 104 (2003).
12. M. Sharon, K. Ramaiah, M. Kumar, M. Neumann-Spallart, C. Levy-Clement, *J. Electroanal. Chem.*, **436**, 49 (1997).
13. Y. J. Yang, *Materials Science and Engineering: B*, **131**, 200 (2006).
14. Y. J. Yang, L. Y. He and Q. F. Zhang, *Electrochem. Commun.*, **7**, 361 (2005).
15. Y. Mikhlin, A. Kuklinskiy, E. Mikhlina, V. Kargin I. Asanov, *J. Appl. Electrochem.*, **34**, 37 (2004).
16. E. E. Stansbury, R. A. Buchanan, Fundamentals of electrochemical corrosion, ASM International, 2000.
17. B. M. Rosales, M. Iannuzzi, *Mater. Sci. Eng.: A*, **472**, 15 (2008).
18. S.-I. Pyun, K.-H. Na, W.-J. Lee, J.-J. Park, *Corrosion*, **56**, 1015 (2000).
19. R. Newman and M. Ajjawi, *Corrosion Sci.*, **26**, 1057 (1986).
20. M. A. Amin, S. S. Abdel Rehim, *Electrochimica Acta*, **49**, 2415 (2004).
21. M. El-Naggar, *J. Mater. Sci.*, **39**, 2747 (2004).
22. P. Veluchamy, M. Sharon, H. Minoura, Y. Ichihashi, K. Basavaswaran, *J. Electroanal. Chem.*, **344**, 73 (1993).
23. J. Galvele, *Corrosion Sci.*, **47**, 3053 (2005).
24. A. Montaser, P. Veluchamy, H. Minoura, *J. Electroanal. Chem.*, **419**, 47 (1996).
25. C. Chao, L. Lin, D. Macdonald, *J. Electrochem. Soc.*, **128**, 1187 (1981).
26. S. M. Sayyah, S. S. Abd-Elrehim, R. E. Azooz, F. Mohamed, *J. Korean Chem. Soc.*, **58,** 24 **(**2014).
27. A. J. Bard, L. R. Faulkner, Electrochemical methods: fundamentals and applications, Wiley New York, 1980.
28. S. Saidman, J. Bessone, *J. Electroanal. Chem.*, **521**, 87 (2002).
29. M. A. Amin, *Electrochimica Acta*, **54**, 1857 (2009).
30. D. Li, P. P. Conway, C. Liu, *Corrosion Sci.*, **50**, 995 (2008).
31. Q. Wang, J.-E. Moser, M. Grätzel, *The J. Physi. Chem. B*, **109**, 14945 (2005).
32. M. Jafarian, F. Gobal, I. Danaee, R. Biabani, M. Mahjani, *Electrochimica Acta*, **53**, 4528 (2008).
33. M. Lashgari, M.-R. Arshadi, S. Miandari, *Electrochimica Acta*, **55**, 6058 (2010).
34. J.-L. Trompette, L. Massot, L. Arurault, S. Fontorbes, *Corrosion Sci.*, **53**, 1262 (2011).
35. K. D. Collins, G. W. Neilson, J. E. Enderby, *Biophysical Chem.*, **128**, 95 (2007).
36. M. Alvarez, J. Galvele, Shreir's Corrosion, Elsevier, Oxford, 2010, p.772.